Orbital Domain Dynamics in Magnetite below the Verwey Transition

Roopali Kukreja,[1,2,3,*] Nelson Hua,[1,2,†] Joshua Ruby,[1] Andi Barbour,[4] Wen Hu,[4] Claudio Mazzoli,[4] Stuart Wilkins,[4] Eric E. Fullerton,[2] and Oleg G. Shpyrko[1,2,‡]

[1]*Department of Physics, University of California, San Diego, La Jolla, California, 92093, USA*
[2]*Center for Memory and Recording Research, University of California, San Diego, La Jolla, California, 92093, USA*
[3]*Department of Materials Science Engineering, University of California, Davis, Davis, California, 95616, USA*
[4]*National Synchrotron Light Source II, Brookhaven National Laboratory, Upton, New York 11973, USA*

(Received 27 March 2018; revised manuscript received 6 July 2018; published 22 October 2018)

The metal-insulator phase transition in magnetite, known as the Verwey transition, is characterized by a charge-orbital ordering and a lattice transformation from a cubic to monoclinic structure. We use x-ray photon correlation spectroscopy to investigate the dynamics of this charge-orbitally ordered insulating phase undergoing the insulator-to-metal transition. By tuning to the Fe L_3 edge at the $(00\frac{1}{2})$ superlattice peak, we probe the evolution of the Fe t_{2g} orbitally ordered domains present in the low temperature insulating phase and forbidden in the high temperature metallic phase. We observe two distinct regimes below the Verwey transition. In the first regime, magnetite follows an Arrhenius behavior and the characteristic timescale for orbital fluctuations decreases as the temperature increases. In the second regime, magnetite phase separates into metallic and insulating domains, and the kinetics of the phase transition is dictated by metallic-insulating interfacial boundary conditions.

DOI: 10.1103/PhysRevLett.121.177601

Mesoscale phenomena play an important role in the dynamics of phase transitions in strongly correlated electron systems. In addition to the coupling of charge, spin, orbital, and lattice degrees of freedom, the underlying mechanism of phase transformations is influenced by nanoscale heterogeneities such as local strain fields, phase separation, domain walls, and defects [1–3]. In order to fully understand and tailor the nanoscale functionalities across metal-insulator phase transitions, detailed access to the nanoscale regime, correlation length scales, and temporal evolution of the order parameter is required. We focused on one such correlated system, magnetite (Fe_3O_4), which shows a metal-insulator transition at $T_V = 123$ K (bulk) [4–9]. It is a model system to study the metal-insulator transition in a much larger group of oxide materials such as manganites and nickelates as the spin system does not undergo any changes during the transition, allowing a focus on electronic and lattice degrees of freedom. The crystal structure of magnetite undergoes a lattice transformation from cubic ($a = b = c = 8.387$ Å) to monoclinic ($a = b = 11.88$ Å, $c = 16.775$ Å and $\beta = 90.236°$) below T_V [7]. Associated with this lattice transformation is a freezing of electronic fluctuations that result in a charge and orbitally ordered low-temperature state, with a conductivity drop of 2 orders of magnitude [4]. Despite the significant amount of research performed over the past 70 years to understand the mechanisms behind the Verwey transition, the role of mesoscale correlations, domain dynamics, and fluctuations of the electronic and lattice system, still remain open questions.

In this Letter, we used x-ray photon correlation spectroscopy (XPCS) to investigate collective dynamics in magnetite due to orbital ordering below the Verwey transition. With recently developed higher brilliance coherent synchrotron sources, this technique allows us to capture coherent speckle patterns arising from the orbitally ordered domains. In general, speckle patterns originate from the presence of disorder in the sample such as domains, defects, and phase separation, and can be considered a fingerprint of the nanoscale heterogeneities present in the sample. Specifically, by measuring the temporal evolution of this speckle pattern at the Fe L_3 edge for the $(00\frac{1}{2})$ superlattice reflection, we can directly probe the t_{2g} orbitally ordered domains in magnetite and shed light on the underlying role of nanoscale heterogeneities in driving the phase transition [10–12]. We reveal two distinct regimes below the Verwey transition. The first regime is characterized by an Arrhenius trend where fluctuations in the orbital order increase as a function of increasing temperature, yet the system remains insulating. In the second regime, the phase separation into metallic and insulating domain occurs, and the kinetics is governed by the interfacial energy between insulating and metallic domains. A slowdown of orbital fluctuations is observed which is attributed to pinning by the insulating or metallic interface. Our studies show that the evolution of orbital fluctuations results in a two-step mechanism for thermally driven phase transition in magnetite.

Magnetite thin films (50 nm) were epitaxially grown by reactive sputtering in Ar/O_2 environment on MgO(001)

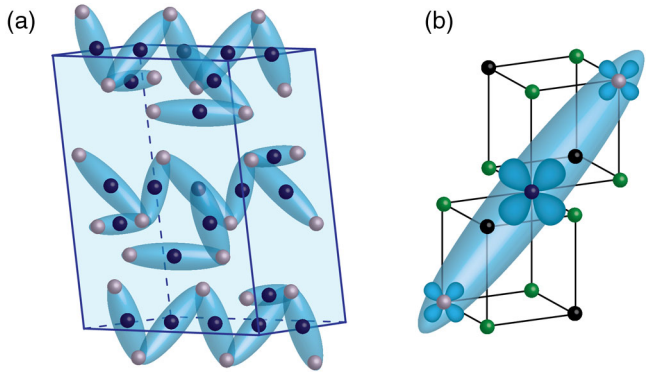

FIG. 1. (a) Monoclinic unit cell of magnetite with trimerons representing the electronic order and lattice distortions. (b) Charge and orbital ordering associated with the trimeron, three-site lattice distortion, where Fe^{2+} (blue) sits at the center of the trimeron, Fe^{3+} (gray) atoms sit at the apex of the trimeron, and green atoms are oxygen [10].

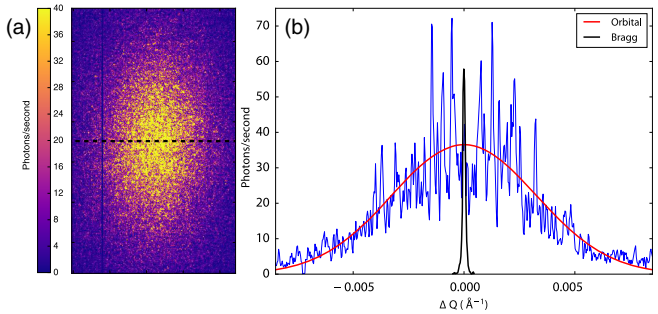

FIG. 2. (a) CCD image of the speckle pattern from the $(00\frac{1}{2})$ superlattice reflection measured at 27 K, (b) Speckle degree of contrast obtained from a line cut through the central speckle pattern in (a). A Gaussian function was fitted to this line cut in order to obtain correlation lengths of the insulating domains. The (001) Bragg reflection (scaled down by 7.5x) is superimposed to illustrate the difference in the structural and orbital correlation lengths as defined by $1/\Delta Q$ of the FWHM.

substrate. The oxygen partial pressure during deposition was 0.1 mTorr and the total deposition pressure was 2 mTorr. Prior to deposition, MgO substrates were heated for 45 min at 500 °C to ensure a good film-substrate interface. The $Fe_3O_4(001)$ films were characterized using x-ray diffraction, and the metal-insulator transition was observed in resistivity measurements (see Supplemental Material [13]). The Verwey transition temperature was found to be $T_V = 116$ K, which is lower than its bulk counterpart and is in good agreement with previously reported values for thin films grown on MgO(001) substrates [14,15]. The low temperature insulating phase has a monoclinic crystal structure, and has been recently described as consisting of a trimeron network where a trimeron is a three-site lattice distortion with a Fe^{2+} atom at the center and two Fe^{3+} atoms at the apex, as shown in Fig. 1[10]. The trimeron represents both the electronic (charge and orbital) and lattice ordering that can be considered as the microscopic entity describing the insulating phase of magnetite. Above T_V, the trimeron order melts, and magnetite transforms into a metallic phase with a cubic crystal structure.

The XPCS experiments were conducted at the coherent soft x-ray scattering (CSX) beam line at the National Synchrotron Light Source II. A coherent beam of photons tuned to the Fe L_3 edge was used to access the $(00\frac{1}{2})$ superlattice reflection. This reflection is forbidden in both the cubic metallic phase and the low temperature monoclinic phase [11,16] and can only be accessed resonantly at the Fe L edge, which allows for a direct probe of the t_{2g} orbitally ordered state of the insulating phase. A coherent beam size of 2 μm was achieved using a 10-μm pinhole in front of the sample, and the scattered beam was recorded with an area detector located 34 cm away from the sample with a 30 μm $\times$ 30 μm pixel size. When coherent x rays scatter from various inhomogeneities present in the magnetite sample, they undergo constructive and destructive interference resulting in a speckle pattern at the detector. This speckle pattern measured in k space is a fingerprint of the sample in real space. These characteristic speckle patterns were recorded as a function of time for various temperatures on the heating cycle of the hysteresis curve starting from 27 up to 110 K, near T_V. An example of a speckle pattern measured at $T = 27$ K is shown in Fig. 2(a). As XPCS probes the disorder in a system, the speckles overlaying the peak in Fig. 2(a) are a direct result of the inhomogeneity of the orbital domains present in the magnetite sample. The speckle contrast is visually represented in Fig. 2(b) as the line cut through the central speckle pattern, which is directly related to the degree of coherence of the x-ray beam and the signal from the system, which comes from the orbitally ordered domains in magnetite. Figure 2(b) also compares the orbital order peak with the structural (001) Bragg peak observed nonresonantly at 800 eV. The observed differences are due to different length scales associated with orbital and structural ordering and are discussed in detail below.

The underlying dynamics in the sample manifests itself as fluctuations of this speckle pattern. In order to investigate these fluctuations, Fig. 3(a) shows "waterfall" plots or kymographs, which depict the evolution of the speckle pattern as a function of time for three temperatures: 27, 70, and 90 K. These waterfall plots are intensity vs time plots, and show the measured intensity along the line cut indicated by the dotted line in Fig. 2(b). From the kymograph plot for 27 K, it is clear that the observed speckles remain stable throughout the three-hour measurement and no evolution of the speckle pattern is observed, which also demonstrates stability of the measurement setup. On the other hand, for temperatures closer to the Verwey transition, at 70 and 90 K, fluctuations in the speckle pattern are observed with speckles appearing and disappearing as a function of time. These fluctuations in the speckle pattern

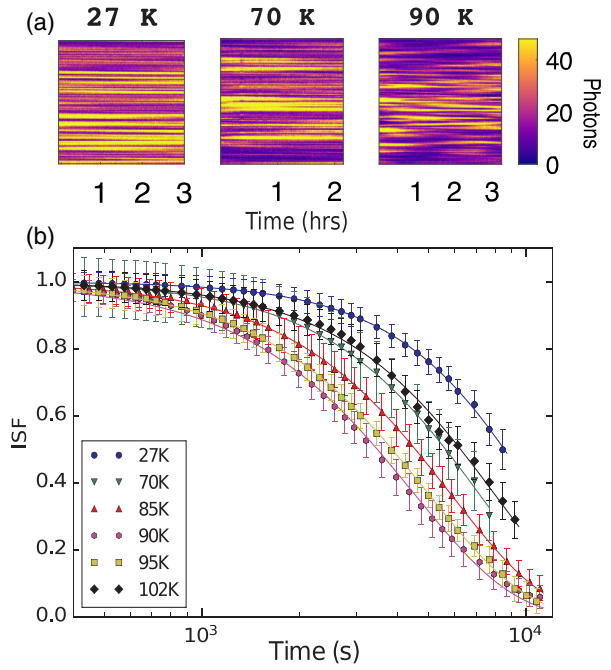

FIG. 3. (a) Kymographs or "waterfall" plots at selective temperatures to demonstrate orbital dynamics in the magnetite film. The waterfall plots are obtained by plotting the central line cut through the speckle pattern shown in Fig. 2(a) as a function of time throughout each scan. (See Supplemental Material [13] for waterfall plots at other temperatures). (b) Intermediate scattering function (ISF) and fits to ISF from Eqs. (1) and (2) are plotted as a function of time for selected temperatures.

are also observed for other temperatures near the Verwey transition (see Supplemental Material [13]) and is direct evidence of orbital domain fluctuations in magnetite below the phase transition.

To quantify the observed dynamics, we calculated the intensity-intensity autocorrelation function $g_2(q,t)$ from the time-dependent speckle measurements described in Eq. (1):

$$g_2(q,t) = \frac{\langle I(q,t)I(q,t+\tau)\rangle}{\langle I(q,t)\rangle^2}, \tag{1}$$

where $I(q,t)$ and $I(q,t+\tau)$ are intensities of a given pixel separated in time by τ, and the $g_2(q,t)$ is calculated from averaging all pixels for a given Δq range of 1.5×10^{-3} Å^{-1} in the speckle pattern. This autocorrelation function calculated from the intensities can be fitted with a stretched exponential as given in Eq. (2):

$$g_2(q,t) = 1 + A\exp^{-2(t/\tau)^{\beta}} = 1 + A|F(q,t)|^2, \tag{2}$$

where A is the speckle contrast, τ is the decay constant, and β is the stretching exponent. The exponential portion is the square of the intermediate scattering function (ISF), $|F(q,t)|^2$, and the temporal evolution of the ISF for temperatures ranging from 27 to 102 K is shown in Fig. 3(b). The ISF value of 1 represents a completely correlated system while 0 represents full decorrelation.

We observe a strong temperature dependence of the ISF, where the timescales decrease as the sample temperature is increased from 27 K to approximately 90 K. However, surprisingly, as the temperature is further increased from 90 to 102 K, an increase in the fluctuation decay time, τ, is observed. We note that no significant q dependence was observed, and hence q dependence was omitted from the g_2 and ISF calculations. Figure 4(a) shows the values obtained for τ and β as a function of temperature. The error bars were calculated using the uncertainty in counting statistics for different q regions. We found the value of the stretching exponent to be greater than 1 ($\beta_{\text{fit}} = 1.5$), manifested by the compressed shape of the ISF. A compressed exponential with $\beta > 1$ represents a collective or jamming behavior where local displacements create long-range inhomogeneities while a value of $\beta < 1$ indicates more liquidlike fluctuations describing spatially

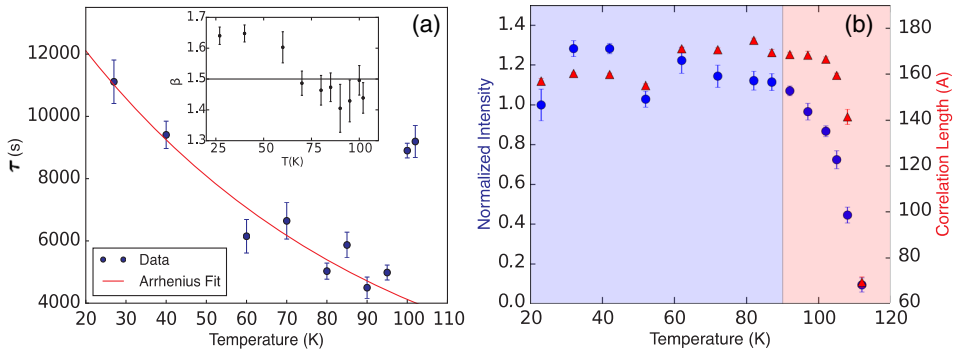

FIG. 4. (a) Characteristic orbital fluctuation timescales as a function of temperature obtained from fits to the intermediate scattering function data shown in Fig. 3(b). An Arrhenius trend (red line) with an activation energy of $\Delta E/k_B = 32 \pm 5$ K is fitted in the first regime (<90 K). Inset shows the fitted stretched exponential value β as a function of temperature that describes the nature of the dynamics. (b) The integrated intensity of the $(00\frac{1}{2})$ peak and the correlation length scales of the insulating domains is calculated from a fitted Gaussian to the central speckle pattern where the correlation length, λ, is $1/\Delta Q$ where ΔQ is the FWHM of the fitted Gaussian peak.

confined dynamics [17,18]. The jamming behavior ($\beta > 1$) is described as ultraslow ballistic motion at large length scales due to elastic relaxation of heterogeneous internal stresses [17]. The obtained fit value of 1.5 in magnetite is considered a universal signature of collective relaxation behavior, and has been previously observed in soft matter systems i.e., gels, sponges, etc., [17,19], materials exhibiting charge density waves [20], and magnetic systems [18].

As observed in the ISF plots, the fluctuation timescales given by τ exhibit a minimum near $T = 90$ K. This nonlinear behavior can be divided into two regimes, (i) below 90 K where the τ decreases as temperature increases and (ii) above 90 K, where τ increases as temperature increases. The first regime was fitted using the standard thermally activated Arrhenius behavior (as shown in Fig. 4(a)) with an activation barrier of $\Delta E/k_B = 32 \pm 5$ K. This activation energy represents the effective energy for orbital domain fluctuations, which grow as more thermal energy is added to the system albeit still significantly below the Verwey temperature. Similar dynamics have been previously observed in other correlated systems such as Cr, manganites, and magnetic systems (Dy and Ho) [17–20]. However, the second regime, where slowdown of fluctuation timescales approaching the transition temperature is observed, cannot be described by the thermally activated behavior.

The temperature dependence of the $(00\frac{1}{2})$ reflection is shown in Fig. 4(b) and its variation across the Fe L_3 edge is shown in the Supplemental Material, Fig. S2 [13]. Correlation lengths of the orbital domains plotted as a function of temperature are shown in Fig. 4(b). The correlation length was obtained from a fitted Gaussian peak [as shown in Fig. 2(b)] of the central speckle pattern, with the correlation length (λ) defined as $1/\Delta Q$ where ΔQ is the full width at half maximum (FWHM) of the fitted Gaussian. The observed FWHM at 27 K is 6.4×10^{-3} Å^{-1} resulting in a correlation length scale of 15.7 nm, which represents the average size of domains with a visible impact on the speckle pattern. The estimated value of orbital ordering correlation length is an order of magnitude lower than lattice ordering correlation length scales and is similar to previously observed values in bulk magnetite of 11–37 nm [11,21]. The difference in correlation length scales from the orbital and structural ordering indicates higher levels of disorder in orbital ordering. Although the origin of lower values of orbital ordering length scales is still not well understood, strain effects, internal defects and doping have been suggested to play a key role [22,23]. For magnetite, it has been interpreted as a signature of disorder in orbital occupancy of t_{2g} orbitals by the Fe^{2+} electron [11,12]. Similar values of orbital correlation length scales have been observed in manganite systems (~30 nm), where it is associated with the orbital glasslike state existing on a well-ordered lattice of charge order [22–24].

By combining the peak intensity, correlation timescales, and length scales, we can now describe the underlying process behind the insulator-to-metal transition. In the first regime (below 90 K), as more thermal energy is injected into the system, the fluctuations in orbital order increase and therefore, a decrease in fluctuation timescale is observed with increasing temperature. The peak intensity stays almost constant, indicating that the system is still insulating. Once the fluctuations achieve a critical energy (near 90 K), the system enters into a second regime and the phase transformation begins. In the second regime (above 90 K), τ increases as the temperature increases, and the thermally activated Arrhenius behavior breaks down. The peak intensity decreases, indicating a reduction in the amount of insulating phase. This implies a transformation of insulating state to metallic state, which significantly changes the boundary conditions of the remaining insulating domains consisting of an orbitally ordered trimeron network. This is also consistent with the observed decrease in correlation lengths of orbitally ordered domains from 17 nm to 6 nm with a normalized integrated peak intensity drop of 80% to 10% near 100 K. In this phase separation regime, the metallic/insulating interface leads to the pinning of the trimeron chains, resulting in a slowdown of orbital fluctuation timescales. Pinning of charge density waves by an interface has been previously observed in other correlated systems [25]. Furthermore, the requirement of relaxation of the monoclinic tilt to transform into the metallic phase can lead to strain at the metallic-insulating interface. Hence, as the system transforms towards the metallic phase, these combined effects of phase separation result in slower fluctuation dynamics. The phase separation into metallic and insulating domains has also been previously observed in single crystal magnetite where the correlation length scales decreased by ~40% with a timescale of 1.5 ps in an optically driven Verwey transition [26]. The presence of phase separation near the Verwey transition in both thin-film magnetite, observed here, and in single-crystal magnetite [26] is evidence of an intrinsic mechanism in magnetite.

Above 116 K, the speckles completely disappear, indicating a complete transformation to the metallic phase. This transition temperature observed at the $(00\frac{1}{2})$ reflection matches well with the conductivity data (Fig. S1 in supplemental Material [13]) and reported for other thin films [15]. Recent studies have also investigated the effects of stoichiometry, film thickness, and choice of substrate on thin-film magnetite compared to bulk magnetite on the nature of the Verwey transition. They show that above a particular value of oxygen partial pressure (1×10^{-7} mbar) during growth and above a particular film thickness (5 nm), a first order Verwey transition is always observed, regardless of the exact T_V or the shape of the hysteresis curve. The exact values for the transition is characterized by the average domain size, which is defined by the film thickness and choice of substrate in the case of thin-films [27,28]. Single crystal magnetite is also defined by its domain size,

and falls within the expected trend in those studies. Thus, while the exact temperature separating the two regimes and the activation energy in the first regime may differ between thin film and bulk samples, the characteristic trends in the fluctuation timescales of the observed orbital order should not vary.

In summary, our XPCS measurements shed light on the transformation pathway of the metal-insulator phase transition in magnetite and show that it proceeds by phase separation. We show that the Verwey transition occurs in a two-step process. The first regime observed below 90 K is ascribed to an Arrhenius behavior where faster orbital fluctuation timescales are observed as the temperature is increases. The second regime is associated with the phase separation into metallic and insulating domains. The characteristic timescale in this regime decreases as the temperature is increased due to the onset of metallic domains as indicated by the drop in peak intensity and correlation length, resulting in interfacial pinning of the orbitally ordered domains in a matrix of metallic domains. This picture is further supported by finding the stretching exponential to be greater than 1 ($\beta \sim 1.5$), suggesting a correlated behavior of the orbital order below the phase transition as it undergoes thermal fluctuations similar to other soft matter systems, Cr, and magnetic systems [17–20]. While the concept of a jamming transition is new to metal-insulator correlated electron materials, the universality of the stretching exponential shows an underlying connection between the fluctuations observed in soft matter systems to the fluctuations observed in the orbitally ordered trimeron network in magnetite.

Sample growth and transport measurements were supported by NSF Grant No. DMR-1411335. Characterization was supported by the AFOSR Grant No. FA9550-16-1-0026 and a University of California collaborative Grant No. MRPI MR-15-328-528. Synchrotron Coherent X-ray Scattering studies were supported by U.S. Department of Energy, Office of Science, Office of Basic Energy Sciences, under Contract No. DE—SC0001805. This research used resources from the 23-ID-1 Coherent Soft X-Ray Scattering (CSX) beam line of the National Synchrotron Light Source II, a U.S. Department of Energy (DOE) Office of Science User Facility operated for the DOE Office of Science by Brookhaven National Laboratory under Contract No. DE-SC0012704.

*Corresponding author.
rkukreja@ucdavis.edu
†nehua@ucsd.edu
‡oshpyrko@physics.ucsd.edu

[1] J. A. Sulpizio, S. Ilani, P. Irvin, and J. Levy, Annu. Rev. Mater. Res. **44**, 117 (2014).
[2] J. H. Ngai, F. J. Walker, and C. H. Ahn, Annu. Rev. Mater. Res. **44**, 1 (2014).
[3] A. Bhattacharya and S. J. May, Annu. Rev. Mater. Res. **44**, 65 (2014).
[4] E. J. W. VERWEY, Nature (London) **144**, 327 (1939).
[5] M. Iizumi and G. Shirane, Solid State Commun. **17**, 433 (1975).
[6] S. Iida, K. Mizushima, M. Mizoguchi, J. Mada, S. Umemura, J. Yoshida, and K. Nakao, Physica (Amsteram) **86–88B+C**, 957 (1977).
[7] M. Iizumi, T. F. Koetzle, G. Shirane, S. Chikazumi, M. Matsui, and S. Todo, Acta Crystallogr. Sect. B **38**, 2121 (1982).
[8] V. I. Anisimov, I. S. Elfimov, N. Hamada, and K. Terakura, Phys. Rev. B **54**, 4387 (1996).
[9] J. P. Wright, J. P. Attfield, and P. G. Radaelli, Phys. Rev. B **66**, 214422 (2002).
[10] M. S. Senn, J. P. Wright, and J. P. Attfield, Nature (London) **481**, 173 (2012).
[11] J. Schlappa, C. Schüßler-Langeheine, C. F. Chang, H. Ott, A. Tanaka, Z. Hu, M. W. Haverkort, E. Schierle, E. Weschke, G. Kaindl, and L. H. Tjeng, Phys. Rev. Lett. **100**, 026406 (2008).
[12] S. B. Wilkins, S. Di Matteo, T. A. W. Beale, Y. Joly, C. Mazzoli, P. D. Hatton, P. Bencok, F. Yakhou, and V. A. M. Brabers, Phys. Rev. B **79**, 201102 (2009).
[13] See Supplemental Material at http://link.aps.org/supplemental/10.1103/PhysRevLett.121.177601 for characterization data on magnetite thin films and waterfall plots.
[14] D. Margulies, F. Parker, F. Spada, and R. Goldman, Phys. Rev. B **53**, 9175 (1996).
[15] G. Q. Gong, A. Gupta, G. Xiao, W. Qian, and V. P. Dravid, Phys. Rev. B **56**, 5096 (1997).
[16] A. Tanaka, C. F. Chang, M. Buchholz, C. Trabant, E. Schierle, J. Schlappa, D. Schmitz, H. Ott, P. Metcalf, L. H. Tjeng, and C. Schüßler-Langeheine, Phys. Rev. Lett. **108**, 227203 (2012).
[17] L. Cipelletti, L. Ramos, S. Manley, E. Pitard, D. A. Weitz, E. E. Pashkovski, and M. Johansson, Faraday Discuss. **123**, 237 (2003).
[18] S. W. Chen, H. Guo, K. A. Seu, K. Dumesnil, S. Roy, and S. K. Sinha, Phys. Rev. Lett. **110**, 217201 (2013).
[19] R. Bandyopadhyay, D. Liang, H. Yardimci, D. A. Sessoms, M. A. Borthwick, S. G. J. Mochrie, J. L. Harden, and R. L. Leheny, Phys. Rev. Lett. **93**, 228302 (2004).
[20] O. G. Shpyrko, E. D. Isaacs, J. M. Logan, Y. Feng, G. Aeppli, R. Jaramillo, H. C. Kim, T. F. Rosenbaum, P. Zschack, M. Sprung, S. Narayanan, and A. R. Sandy, Nature (London) **447**, 68 (2007).
[21] J. E. Lorenzo, C. Mazzoli, N. Jaouen, C. Detlefs, D. Mannix, S. Grenier, Y. Joly, and C. Marin, Phys. Rev. Lett. **101**, 226401 (2008).
[22] K. J. Thomas, J. P. Hill, S. Grenier, Y. J. Kim, P. Abbamonte, L. Venema, A. Rusydi, Y. Tomioka, Y. Tokura, D. F. McMorrow, G. Sawatzky, and M. Van Veenendaal, Phys. Rev. Lett. **92**, 237204 (2004).
[23] J. J. Turner, K. J. Thomas, J. P. Hill, M. A. Pfelfer, K. Chesnel, Y. Tomioka, Y. Tokura, and S. D. Kevan, New J. Phys. **10**, 053023 (2008).
[24] J. P. Hill, C. S. Nelson, M. V. Zimmermann, Y. J. Kim, D. Gibbs, D. Casa, B. Keimer, Y. Murakami, C. Venkataraman, T. Gog, Y. Tomioka, Y. Tokura, V. Kiryukhin, T. Y. Koo, and S. W. Cheong, Appl. Phys. A **73**, 723 (2001).

[25] A. Singer, S. K. K. Patel, V. Uhlíř, R. Kukreja, A. Ulvestad, E. M. Dufresne, A. R. Sandy, E. E. Fullerton, and O. G. Shpyrko, Phys. Rev. B **94**, 174110 (2016).
[26] S. de Jong *et al.*, Nat. Mater. **12**, 882 (2013).
[27] X. H. Liu, A. D. Rata, C. F. Chang, A. C. Komarek, and L. H. Tjeng, Phys. Rev. B **90**, 125142 (2014).
[28] X. Liu, C.-F. Chang, A. D. Rata, A. C. Komarek, and L. H. Tjeng, npj Quantum Mater. **1**, 16027 (2016).